Cellular Entry of Lymphocytic Choriomeningitis Virus[▽][†]

Jillian M. Rojek,[1] Mar Perez,[2] and Stefan Kunz[1]*

*Molecular and Integrative Neurosciences Department, The Scripps Research Institute, La Jolla, California 92037,[1]
and Centro Nacional de Investigaciones Oncológicas, Melchor Fernández Almagro, 3, 28029 Madrid, Spain[2]*

In contrast to most enveloped viruses that enter the host cell via clathrin-dependent endocytosis, the Old World arenavirus lymphocytic choriomeningitis virus (LCMV) enters cells via noncoated vesicles that deliver the virus to endosomes, where pH-dependent membrane fusion occurs. Here, we investigated the initial steps of LCMV infection. We found that the attachment of LCMV to its cellular receptor α-dystroglycan occurs rapidly and is not dependent on membrane cholesterol. However, subsequent virus internalization is sensitive to cholesterol depletion, indicating the involvement of a cholesterol-dependent pathway. We provide evidence that LCMV entry involves an endocytotic pathway that is independent of clathrin and caveolin and that does not require the GTPase dynamin. In addition, neither the structural integrity nor the dynamics of the actin cytoskeleton are required for infection. These findings indicate that the prototypic Old World arenavirus LCMV uses a mechanism of entry that is different from clathrin-mediated endocytosis, which is used by the New World arenavirus Junin virus, and pathways used by other enveloped viruses.

Arenaviruses provide powerful experimental models to understand viral pathogenesis as well as being important human pathogens (8). Infection of the prototypic Old World arenavirus, lymphocytic choriomeningitis virus (LCMV), in its natural host, the mouse, has illuminated numerous fundamental concepts in virology and immunology that have been extended to other viruses and pathogens (50). LCMV also is an important pathogen in human pediatric medicine (32) and recently has been implicated in lethal infections of transplantation patients (24). The related Lassa fever virus (LFV) causes a severe hemorrhagic fever in humans, with over 300,000 infections and several thousand deaths per year in Africa (27, 44). The New World arenaviruses Guanarito, Junin, Machupo, and Sabia have emerged as causative agents of severe hemorrhagic fevers in the Americas. Currently there is neither an efficient vaccine nor efficacious treatment for human Old World arenavirus infections, and novel therapeutic approaches are needed to combat these pathogens. Thus, understanding the arenavirus life cycle and virus-host cell interaction is crucial for the development of potent antiarenaviral strategies.

Arenaviruses are enveloped single-strand RNA viruses with a bisegmented genome in an ambisense organization (8). Their genome consists of a large RNA segment encoding the virus polymerase (L) and a small zinc finger motif protein (Z), as well as a smaller RNA segment encoding the virus nucleoprotein (NP) and glycoprotein (GP) precursor. The GP precursor is processed into peripheral GP1 and transmembrane GP2. GP1 is implicated in receptor binding (6), and GP2 is structurally similar to the fusion-active membrane-proximal portions of other enveloped viruses (23, 26).

Viral entry is the first step of every virus infection and represents an important target for combating viruses before they can gain control over the host cell machinery for replication (31, 41, 42, 69). The cellular receptor for LCMV and LFV is α-dystroglycan (α-DG), a cell surface receptor for proteins of the extracellular matrix (2, 10, 70). Upon initial attachment to the target cell, LCMV virions are taken up in smooth-walled vesicles that are not associated with clathrin (7). The New World arenaviruses Guanarito, Junin, Machupo, and Sabia can use human transferrin receptor 1 as a cellular receptor (58), and clathrin-dependent endocytosis has been reported for the entry of Junin virus (43). Following internalization, arenavirus-containing vesicles are acidified as they move through the cell. Fusion of the viral membrane with the vesicle membrane is triggered as the pH drops to 5.3 to 5.5, corresponding to the pH of late endosomes (7, 11, 18, 19, 80). As is the case for fusion-active GPs of other enveloped viruses, low pH is thought to trigger conformational changes in the arenavirus GP that result in the exposure of a fusion peptide that can mediate the fusion of the virion and host cell membranes (23, 26).

It is now widely accepted that animal viruses can use clathrin-independent pathways for endocytosis. The best studied are cholesterol-dependent pathways involved in the entry of an increasing number of enveloped and nonenveloped viruses (3, 12, 14, 16, 53, 54, 57, 71, 75). Recently, it was demonstrated that the depletion of cholesterol from murine embryonic stem cells inhibited infection with LCMV, suggesting a role for membrane cholesterol in one or more steps of LCMV infection (66).

MATERIALS AND METHODS

Proteins and antibodies. α-DG was purified from mouse tissues as reported previously (45). Natural mouse laminin-1 was obtained from Invitrogen. Monoclonal antibodies (MAbs) 113 (anti-LCMV NP) as well as 36.1 and 83.6 (anti-LCMV GP) have been described previously (9, 77), as have MAb 10G4 (anti-VSV NP), MAb I1 (anti-VSV GP) (40), and MAb IIH6 (anti-α-DG) (22). Mouse hyperimmune serum against New World arenaviruses was kindly provided by Christina F. Spiropoulou, Special Pathogens Branch, Centers for Disease Con-

* Corresponding author. Mailing address: Molecular and Integrative Neurosciences Department, The Scripps Research Institute, 10550 N. Torrey Pines Rd., La Jolla, CA 92037. Phone: (858) 784-9447. Fax: (858) 784-9981. E-mail: stefanku@scripps.edu.

trol and Prevention (Atlanta, GA). Rabbit polyclonal anti-laminin antibody and actin-phalloidin were purchased from Sigma (St. Louis, MO). Rabbit polyclonal antibody to caveolin-1 was obtained from Santa Cruz Biotechnology, and MAb to the simian virus 40 (SV40) large T antigen was purchased from BD Biosciences. Rhodamine X-conjugated and fluorescein isothiocyanate-conjugated secondary antibodies were from Jackson ImmunoResearch (West Grove, PA), and horseradish peroxidase (HRP)-conjugated secondary antibodies were from Pierce (Rockford, IL). 4′,6′-Diamidino-2-phenylindole (DAPI) was from Invitrogen. For immunoprecipitation (IP) experiments, purified MAb 83.6 was conjugated to cyanogen bromide-activated Sepharose 4B as described previously (39).

Cells and viruses. African green monkey kidney (Vero E6) cells were maintained in minimal essential medium (Gibco BRL, NY) containing 7% fetal bovine serum (FBS) and supplemented with glutamine and penicillin-streptomycin. North African green monkey (*Cercopithecus aethiops*) kidney fibroblasts (CV1) (ATCC CCL-70), human cervix carcinoma cells (HeLa), Syrian golden hamster kidney cells (BHK-21), and human hepatocyte line Huh7 (46, 47) were maintained in Dulbecco's modified essential medium (DMEM) (Gibco BRL, NY) containing 10% FBS and supplemented with nonessential amino acids, glutamine, and penicillin-streptomycin.

Seed stocks of LCMV were prepared by growth in BHK-21 cells, and titers were determined as reported previously (21). The origin, passage, and characteristics of LCMV clone 13 (cl-13) have been described already (1). Wild-type vesicular stomatitis virus (VSV) (Indiana serotype) and recombinant VSV containing a green fluorescent protein (GFP) reporter (rVSV-GFP) were provided by Juan-Carlos de la Torre (The Scripps Research Institute), and the Junin virus Candid 1 vaccine strain was provided by Michael Buchmeier (TSRI). Junin virus Candid 1 was grown in Vero E6 cells, and titers were determined by plaque assay (21). VSV and rVSV-GFP stocks were grown in Vero E6 cells, and titers were determined by plaque assay on Vero E6 cells. SV40 obtained from the ATCC was grown in CV1 cells, and the titers of virus stocks were determined as described previously (53).

Recombinant VSV pseudotyped with LFV GP, LCMV cl-13 GP, or VSV GP was generated as reported previously (35). Virus titers were determined by the infection of Vero E6 cell monolayers and detection of GFP-positive cells by fluorescence microscopy. Titers of pseudotypes were expressed as infectious units.

Generation of recombinant VSV containing the GP of LCMV cl-13. To generate rVSV-LCMV GP, the open reading frame (ORF) of LCMV GP was amplified from the pC-LCMV cl-13 GP with primers 5′-CGA CGC GTT GAC ACT ATG GGT CAG ATT GTG ACA ATG-3′ and 5′-CTA GCT AGC TCA GCG TCT TTT CCA GAC GGT TTT TAC ACC-3′ and was cloned into the MluI and NheI sites (corresponding sites in the primers are underlined) of the pVSVΔG-PL vector (59), in which the VSV GP ORF had been replaced by an oligonucleotide-derived polylinker region (5′-MluI-KpnI-XhoI-SmaI-EagI-SphI-NheI-3′). The infectious virus was rescued by following well-established protocols (59, 65, 74). Briefly, BHK-21 cells were infected with vTFT7.3, a recombinant vaccinia virus expressing the phage T7 RNA polymerase (25). After 1 h, plasmids encoding VSV NP, P, GP, and L proteins were cotransfected together with the full-length cDNA clone of the VSV genome (Indiana serotype) containing LCMV GP Armstrong cl-13 as an additional VSV ORF. The supernatant fluid was harvested 48 h after transfection, filtered to remove vTFT7.3, and used to infect BHK-21 cells *trans*-complemented with VSV GP to enhance the efficiency of virus rescue. Cells were examined for cytopathic effect and VSV NP expression 24 h after infection to assess virus rescue. The virus recovered from this second infection was plaque purified three times in BHK-21 cells expressing VSV GP and then passaged three times on Vero E6 cells to ensure that the viral preparation was cleaned of VSV GP. The LCMV GP gene in rVSVΔG-LCMV GP was sequenced and found to be identical to the parental LCMV cl-13 GP gene. The virus was propagated on Vero E6 cells, and infectivity was quantified using a Vero E6 cell plaque assay.

Detection of arenavirus GP incorporated into retroviral pseudotypes. For the detection of the GPs of LCMV and VSV in LCMV cl-13, rVSV-LCMV GP, and VSV, purified viruses (10^7 PFU/ml in phosphate-buffered saline [PBS]) were coated in triplicate wells in 96-well enzyme immunoassay/radioimmunoassay high-bond microtiter plates (Corning) for 2 h at 6°C; nonspecific binding was blocked with 1% (wt/vol) bovine serum albumin (BSA)–PBS. For the detection of LCMV GP, MAbs 36.1 (anti-GP1) and 83.6 (anti-GP2) were applied at 20 μg/ml, and MAb I1 (anti-VSV GP) was used at 2 μg/ml. The incubation was for 2 h at 6°C, and bound primary antibodies were detected with HRP-conjugated anti-mouse immunoglobulin G (IgG) (1:1,000) in a color reaction using ABTS [2,2′azino-bis(3-ethylbenzthiazoline-6-sulfonic acid] substrate. The optical density at 405 nm was measured with an enzyme-linked immunosorbent assay

(ELISA) reader. For the determination of specific binding, background binding to BSA was subtracted.

Virus infection of cells. For the infection of cells with LCMV cl-13, rVSV-LCMV GP, VSV, and rVSV-GFP, seed stocks were diluted to the indicated multiplicity of infection (MOI) and were added to cells for 1 h at 37°C. After 1 h of incubation at the indicated temperature, inoculum was removed, cells were washed twice with medium without serum, and cells were incubated for the indicated time periods at 37°C and 5% CO_2. Infection was quantified by immunofluorescence detection of LCMV NP and VSV NP using MAbs 113 (anti-LCMV NP) and 10G4 (anti-VSV NP) combined with fluorescence-labeled secondary antibodies (10). Quantification of LCMV infection by flow cytometry was performed as reported previously (61).

For blocking experiments with inactivated virus, LCMV cl-13 and VSV were inactivated by UV irradiation (61). Vero E6 cells cultured on 96-well plates (2 × 10^3 cells/well) were incubated with the indicated concentration of inactivated viruses in a total volume of 100 μl/well in 50% OPTIMEM–50% PBS for 2 h on ice. Two hundred plaque-forming units of LCMV cl-13, rVSV-LCMV GP, and VSV then were mixed with the same concentrations of inactivated viruses in a total volume of 100 μl OPTIMEM-PBS, and the inoculum was added to the cells. After 45 min, supernatants were removed and cells were washed three times with medium and incubated for 16 h in the cases of LCMV cl-13 and rVSV-LCMV GP and 6 h in the case of VSV. Infection was quantified by immunofluorescence detection of LCMV NP and VSV NP. The blocking of infection by rVSV-LCMV GP and VSV with soluble α-DG was performed as described previously (38).

Infection and internalization assays with wild-type and DN mutants of caveolin-1, dynamin, and Eps15. Wild-type GFP-caveolin-1 (53) and the GFP-tagged dominant-negative (DN) caveolin-1 mutant cav-1Y14F (14) were provided by Jeffrey M. Bergelson (University of Pennsylvania). GFP-tagged wild-type and DN (K44E) dynamin I and dynamin II (76) were kindly provided by Sandra L. Schmid (TSRI). For the analysis of the clathrin-mediated entry pathway of arenaviruses, the control Eps15DIIIΔ2 construct (5) and the DN Eps15Δ95/295 mutant construct (4) were provided by Alice Daurty-Varsat and Nathalie Sauvonnet (Institut Pasteur, Paris, France). Cells were grown to 50 to 70% confluence in LabTek cell culture chamber slides (Nunc) and transiently transfected with plasmid DNA using Superfect reagent (Qiagen) or the Nucleofector system (Amaxa, Gaithersburg, MD) according to the manufacturer's protocols. Transfection efficiencies with plasmids, as assessed by the detection of GFP, were 40 to 60% depending on the cell type and transfection method used. Cells expressing GFP-tagged constructs for 16 to 20 h were infected with LCMV cl-13 and Junin virus Candid 1 at the indicated MOI as described above and analyzed for the expression of LCMV or Junin antigen after 12 to 16 h by immunofluorescence staining (10). In three independent transfections, at least 100 cells with comparable levels of transgene expression were screened, and cells positive for viral antigen were scored. Fluorescent images were captured using a Zeiss Axiovert S100 microscope (Carl Zeiss Inc., Thornwood, NY) with a ×20 objective and an AxioCam digital camera. Images were assembled using Adobe Photoshop.

Transferrin uptake studies were performed as reported previously (73). Briefly, cells transfected with GFP-tagged constructs for 16 to 20 h were serum starved for 30 min, chilled on ice for 5 min, and incubated with 10 μg/ml Alexa 594-labeled human transferrin (Molecular Probes) in medium supplemented with 20 mM HEPES, pH 7.2. After incubation on ice in the dark for 20 min, cells were shifted to 37°C for 20 min. Cells were chilled on ice, briefly treated with 0.1 M glycine, 150 mM NaCl, pH 4.0, to quench surface fluorescence, and immediately fixed with 2% (wt/vol) paraformaldehyde in PBS for 15 min at room temperature. Specimens were examined by fluorescence microscopy as described above.

Pharmacological inhibitors. For cholesterol extraction with methyl-β-cyclodextrin (MBCD), medium was removed, cells were washed twice with medium without FBS, and MBCD (Fluka) was added at the indicated concentrations for 1 h at 37°C and 5% CO_2. Cells were washed three times with medium to remove residual MBCD, and infection assays were performed as described above. For cholesterol replenishment, cholesterol-loaded MBCD was added to the medium and incubated with the cells for an additional hour (17). The sequestration of membrane cholesterol was achieved by incubation with nystatin (25 μg/ml) and progesterone (10 μg/ml) for 16 h (16). In contrast to MBCD, nystatin and progesterone were present for the duration of the experiment. For the quantitative determination of cellular cholesterol, cells were extracted with chloroform and methanol (2:1), and the amount of cholesterol was quantified by a commercial colorimetric assay (BioVision Inc., Mountain View, CA) according to the manufacturer's recommendations.

Inhibitor drugs to help study the role of the actin cytoskeleton were used at concentrations and for incubation times described previously (14, 16, 54). Cy-

tochalasin D (Sigma) was used at 25 μg/ml, latrunculin A (Calbiochem) at 1 μM, and jasplakinolide (Invitrogen) at 500 nM. Unless indicated otherwise, inhibitors were added at the indicated time points and were present for the duration of the experiment.

Flotation assay and fractionation. Triton X-100 extraction, flotation, and fractionation were done as described previously (29). CV1 and Vero E6 cells cultured in 10-cm tissue culture plates were lysed in lysis buffer (1 ml per dish) containing 1% Triton X-100, 50 mM Tris-HCl, pH 7.5, 150 mM NaCl, 1 mM MgCl$_2$, 1 mM CaCl$_2$ supplemented with 1 mM phenylmethylsulfonyl fluoride (PMSF) and Complete protease inhibitor cocktail for 1 h. Lysates were cleared by centrifugation at 10,000 rpm and 4°C for 10 min and were loaded on a 10, 55, and 63% discontinuous sucrose gradient in a Beckman SW41 Ti rotor. Ultracentrifugation was performed at 37,000 rpm for 16 h at 4°C. After ultracentrifugation, nine fractions (1.5 ml each) were collected from the top (numbered 1 to 9).

Virus binding and internalization assays. LCMV cl-13 was purified twice by ultracentrifugation on a renografin gradient and biotinylated using the reagent N-hydroxysuccinimide (NHS)-X-biotin (Calbiochem) as described previously (38). The infectivity of biotinylated virus was verified by plaque assay on Vero E6 cells, and only preparations that retained >50% infectivity were used for binding. For binding assays, 5 × 10^5 CV1 or Vero E6 cells were cultured per well of M6 plates to obtain closed monolayers. Medium was removed, and cells were washed twice with cold Hanks balanced salt solution (HBSS) and chilled on ice. HBSS was removed, and 1 ml biotinylated LCMV (10^7 PFU/ml in HBSS) was added. After incubation for the indicated time periods on ice, virus was removed, and cells were washed three times with cold HBSS and lysed immediately in 1 ml of lysis buffer/well containing 1% (wt/vol) Triton X-100, 0.05% (wt/vol) sodium dodecyl sulfate (SDS), 50 mM Tris-HCl, pH 7.5, 150 mM NaCl, 1 mM EDTA, 1 mM PMSF, Complete protease inhibitor cocktail (Roche) for 30 min. Lysates were cleared by centrifugation at 12,000 rpm and 4°C for 10 min, and unlabeled purified LCMV (10^7 PFU/ml final concentration) was added as a carrier. For the IP of LCMV GP2, lysates were incubated with 10 μl of MAb 83.6 immobilized on Sepharose 4B (5 μg purified mouse IgG per μl) overnight at 4°C. After four wash steps with lysis buffer, bound LCMV GP2 was eluted by boiling the antibody matrix in SDS-polyacrylamide gel electrophoresis (PAGE) sample buffer for 5 min. IPs were separated by SDS-PAGE, proteins were blotted to nitrocellulose, and biotinylated GP2 was detected by streptavidin-HRP (1:5,000) using SuperSignal West Femto maximum sensitivity substrate (Pierce) and enhanced chemiluminescence (ECL).

The internalization of virus was studied using a modified assay reported earlier for vesicular uptake of cellular ligands (64, 79) and viruses (54). Briefly, purified LCMV was labeled with the thiol-cleavable reagent NHS-SS-biotin (Pierce) (38). The cleavage of the biotin label was verified by treatment with 15 mM of the membrane-impermeable reducing agent Tris(2-carboxyethyl)phosphine (TCEP) (Pierce) for 30 min, which resulted in a loss of >95% of the biotin label.

For internalization assays, CV1 or Vero E6 cells were cultured in 10-cm dishes to obtain closed monolayers. Medium was removed, and cells were washed twice with cold HBSS and chilled on ice for 5 min. Cold solution containing NHS-SS-biotinylated LCMV (10^7 PFU/ml) in HBSS was added. After incubation for 1 h on ice, unbound virus was removed and cells were washed three times with cold HBSS. For internalization, warm medium was added and cells were put on metal blocks in an incubator at 37°C. After the indicated incubation times, medium was removed, cold HBSS was added, and cells were chilled on ice to stop membrane movements. A freshly prepared cold solution of TCEP (15 mM) in 50 mM HEPES, pH 7.5, 150 mM NaCl, 1 mM CaCl$_2$, 1 mM MgCl$_2$ was added (5 ml/dish) and applied twice for 30 min on ice. Cells were washed three times with cold HBSS, and the remaining TCEP was quenched with 100 mM iodoacetamide in 50 mM HEPES, pH 7.5, 150 mM NaCl, 1 mM CaCl$_2$, 1 mM MgCl$_2$ for 10 min, and cells were lysed immediately in lysis buffer (1 ml/dish) for 30 min. LCMV GP2 was isolated by IP as described above. Immunocomplexes were separated by nonreducing SDS-PAGE. Biotinylated LCMV GP2 was detected by Western blotting with HRP-conjugated streptavidin as described above. For quantification, X-ray films were scanned with a Storm densitometer, and acquired data were processed using Image Quant software.

Immunoblotting, laminin overlay assay, and virus overlay assay. Standard immunoblotting involved proteins being separated by SDS-PAGE and transferred to nitrocellulose. After being blocked in 5% (wt/vol) skim milk in PBS, membranes were incubated with 10 μg/ml primary antibody, MAb IIH6 to α-DG, MAb 83.6 (anti-LCMV GP2), and rabbit polyclonal antibody (anti-caveolin-1) in 2% (wt/vol) skim milk, PBS overnight at 6°C. After several washes in PBS, 0.1% (wt/vol) Tween 20 (PBST), secondary antibodies coupled to HRP were applied (1:5,000) in PBST for 1 h at room temperature. Blots were developed using SuperSignal West Pico ECL substrate (Pierce). The laminin overlay assay was

performed as described previously (45), and the virus overlay protein binding assay was performed as described previously (10).

Depletion of caveolin-1 by siRNA. For the depletion of caveolin-1 from CV1 cells, siGENOME ON-TARGETplus SMARTpool duplex (J-003467-06) to human caveolin-1 and a control short interfering RNA (siRNA) pool were obtained from Dharmacon Research (Lafayette, CO). The pool consisted of the following siRNAs: 1, 5′-CUA AAC ACC UCA ACG A<u>U</u>G AUU-3′; 2, 5′-GCA AAU ACG UAG ACU CGG AUU-3′; 3, 5′-GCA GUU GUA CCA UGC AUU AUU-3′; and 4, GCA UCA ACU UGC AGA AAG AUU-3′. siRNAs 2, 3, and 4, targeting human caveolin-1 cDNA (GenBank accession no. NM_001753), perfectly match the corresponding sequences in the caveolin-1 cDNA of *C. aethiops* (GenBank accession no. DP000029), from which CV1 cells are derived. siRNA 1 contains one mismatched U-C base between the human and *C. aethiops* sequences (underlined).

The depletion of caveolin-1 was performed as described previously (63). Briefly, CV1 cells (2 × 10^4 cell/well) were seeded in 96-well plates and transfected with siRNAs at concentrations of 50 nM per siRNA, corresponding to a total concentration of 200 nM, using Lipofectamine 2000. After 48 h, cells were lysed and the depletion of caveolin-1 was detected by Western blot analysis, using α-tubulin for normalization. Parallel samples were infected with LCMV cl-13, Junin virus Candid 1, or SV40 (200 PFU/well). Infections of LCMV cl-13 and Junin virus Candid 1 were assessed by immunofluorescence, as described above. For the detection of SV40 infection, cells were fixed after 16 h and stained with a MAb to the SV40 T antigen combined with a rhodamine red-X-conjugated anti-mouse IgG secondary antibody as reported previously (53, 54). To exclude unwanted off-target effects of siRNA treatment, siRNA pools to caveolin-1 and control siRNA were cotransfected with the luciferase expression construct pEGSH-Luc, and luciferase activity was assessed by a Steady-Glo luciferase assay from Promega (Madison, WI) according to the manufacturer's recommendations. No significant reduction in luciferase activity was observed in cells cotransfected with pEGSH-Luc and caveolin-1 siRNAs or control siRNAs.

RESULTS

Entry of LCMV is dependent on membrane cholesterol. To investigate the early steps of LCMV infection, we chose the prototypic immunosuppressive LCMV isolate cl-13, which binds its cellular receptor α-DG with high affinity and has receptor binding characteristics and cellular tropism similar to those of the related human pathogenic LFV (10, 35, 36, 61). VSV, which uses a cellular receptor(s) different from α-DG (10, 62) and enters cells via a cholesterol-independent, clathrin-dependent pathway (73), was selected as a control. The GP of arenaviruses is necessary and sufficient for the attachment to and entry into target cells. In order to separate LCMV entry from subsequent steps of viral replication, we generated a recombinant VSV that contained the GP of LCMV cl-13 (rVSV-LCMV GP) using VSV reverse genetics (for details, see Materials and Methods).

Compared to that of wild-type VSV, rVSV-LCMV GP showed attenuated growth in Vero E6 cells (Fig. 1A). A similar attenuation has been observed recently with a recombinant VSV containing the GP of Borna disease virus (55). The incorporation of LCMV GP into rVSV-LCMV GP was verified by the detection of the GP1 and GP2 parts of LCMV GP by specific MAbs in an ELISA (Fig. 1B). Based on our ELISA data, the incorporation of LCMV GP into rVSV-LCMV GP was less efficient than that into LCMV cl-13. A similarly reduced efficiency of incorporation of heterologous viral GPs into recombinant VSV has been reported previously (55). The infection of cells by rVSV-LCMV GP was blocked specifically by inactivated LCMV cl-13 but not inactivated VSV (Fig. 1C), and the infection of cells with rVSV-LCMV GP, but not VSV, was strongly inhibited by soluble α-DG (Fig. 1D), indicating
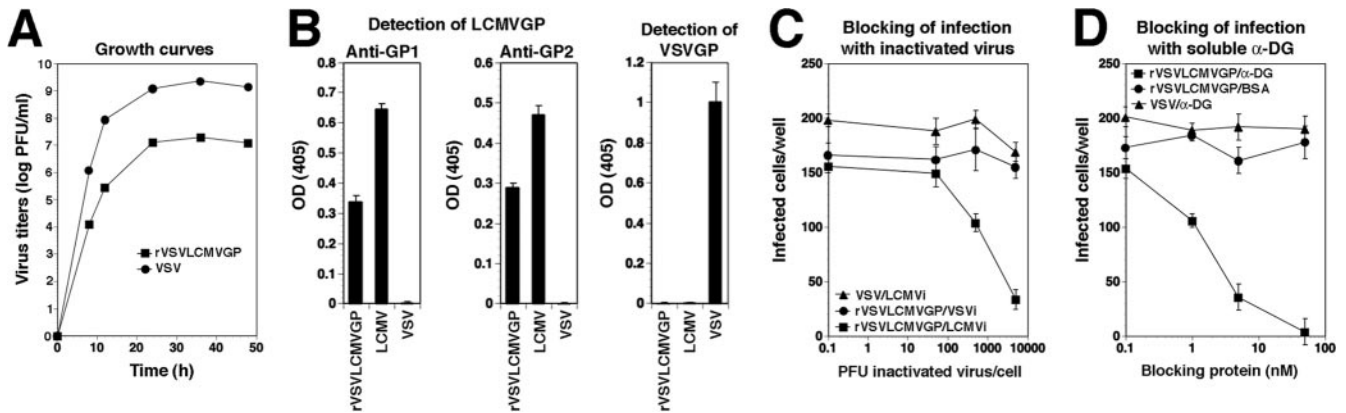
FIG. 1. Recombinant VSV expressing the GP of LCMV cl-13 (rVSV-LCMV GP). (A) Attenuated growth of rVSV-LCMV GP. Vero E6 cells were infected with rVSV-LCMV GP or wild-type VSV (MOI = 1), and virus titers were determined in the supernatants after the indicated time points. (B) Detection of LCMV GP in rVSV-LCMV GP. Immobilized rVSV-LCMV GP, LCMV cl-13, and VSV were probed with MAbs to LCMV GP1, LCMV GP2, and VSV GP in ELISA (n = 3 ± standard deviations). OD(405), optical density at 405 nm. (C) Blocking of rVSV-LCMV GP infection by inactivated LCMV cl-13. Vero E6 cells were blocked with inactivated LCMV cl-13 (LCMVi) or VSV (VSVi) at the indicated ratios of virus particles per cell, followed by infection with 200 PFU of the indicated viruses. Infection was assessed by immunofluorescence staining with MAbs to the corresponding viral NPs after 16 h for LCMV cl-13 and rVSV-LCMV GP and 6 h for VSV. NP-positive cells were scored (n = 3 ± standard deviations). (D) Infection of rVSV-LCMV GP is blocked by soluble α-DG. rVSV-LCMV GP and VSV (200 PFU each) were incubated with the indicated concentrations of soluble α-DG or BSA and added to monolayers of Vero E6 cells. Infection was determined as described for panel C (n = 3 ± standard deviations).

that the rVSV-LCMV GP chimera indeed has the receptor binding characteristics of LCMV cl-13.

Recently, membrane cholesterol has been implicated in LCMV infection (66), although the specific step(s) of virus infection that depended on cholesterol was not identified. To clearly define the role of membrane cholesterol in viral entry, we studied the impact of drugs that either extract or sequester membrane cholesterol on infection with LCMV cl-13 and rVSV-LCMV GP, using VSV as a control.

In a first set of experiments, MBCD, a well-characterized drug that efficiently extracts membrane cholesterol (78), was applied. As cellular models, we used two different primate cell lines, the fibroblast line Vero E6 and the epithelial cell line CV1. Treatment of cells with increasing concentrations of MBCD for 1 h reduced cellular cholesterol levels in a dose-dependent manner (Fig. 2A). To address the impact of cholesterol depletion on virus infection, cells were pretreated with increasing concentrations of MBCD for 1 h, followed by washing out the drug. Cells then were infected with LCMV cl-13, rVSV-LCMV GP, and rVSV-GFP. Infections with LCMV cl-13 and rVSV-LCMV GP were assessed after 16 h by immunofluorescence detection of the NP of LCMV and VSV, which represent the earliest viral gene products. Infection with rVSV-GFP was assessed by direct fluorescence detection of GFP. As shown in Fig. 2B, the depletion of cellular cholesterol resulted in a significant reduction of subsequent infection with LCMV cl-13 and rVSV-LCMV GP, but infection with rVSV-GFP was not reduced. The lack of an effect on infection with rVSV-GFP excludes severe and nonspecific toxicity of the drug. However, since acute cholesterol depletion by MBCD also may affect cholesterol-independent endocytosis (60, 72), we studied the combination of the cholesterol-sequestering drug nystatin and the cholesterol synthesis inhibitor progesterone (16, 54) in a complementary manner. As with our observations with MBCD, preincubation of cells for 16 h with nystatin/proges-

terone resulted in a significant reduction of subsequent infection with LCMV cl-13 and rVSV-LCMV GP, but infection with rVSV-GFP was not reduced (Fig. 2C).

If the effects of MBCD on infection with LCMV cl-13 and rVSV-LCMV GP were due to the removal of cholesterol, the replenishment of cholesterol after MBCD treatment should restore infection. After treatment with 10 mM MBCD for 1 h, cells were allowed to recover either in cholesterol-free medium or in medium supplemented with cholesterol-loaded MBCD (17), which resulted in the nearly complete restoration of cholesterol levels (Fig. 2D). Cholesterol replenishment resulted in a reversal of the inhibitory effect of MBCD on virus infection (Fig. 2E), indicating that cholesterol depletion likely is responsible for the observed inhibition.

To confirm a role of membrane cholesterol in early steps of LCMV infection, cells either were preincubated with MBCD or were treated at different time points postinfection. This approach is based on the fact that MBCD treatment removes membrane cholesterol rapidly, resulting in low cellular cholesterol levels for >6 h, followed by slow recovery (Fig. 2F). While pretreatment with MBCD for 1 h markedly reduced the levels of infection with LCMV cl-13 and rVSV-LCMV GP, the addition of MBCD at later time points had no effect (Fig. 2G), indicating that cholesterol depletion affects an early step of infection.

We next addressed the role of membrane cholesterol in the entry of the related LFV. To overcome biosafety restrictions imposed by the requirement of biosafety level 4 facilities for work with live LFV, we used an established VSV pseudotype system. The GP of LFV (strain Josiah) was incorporated into the surface of recombinant VSV, in which the VSV G gene was replaced by a GFP reporter gene (VSVΔG*) as described previously (35, 56). These pseudotyped VSV particles (VSVΔG*-LFV GP) acquire the receptor binding characteristics of LFV (35). In addition, we generated VSV pseudotypes
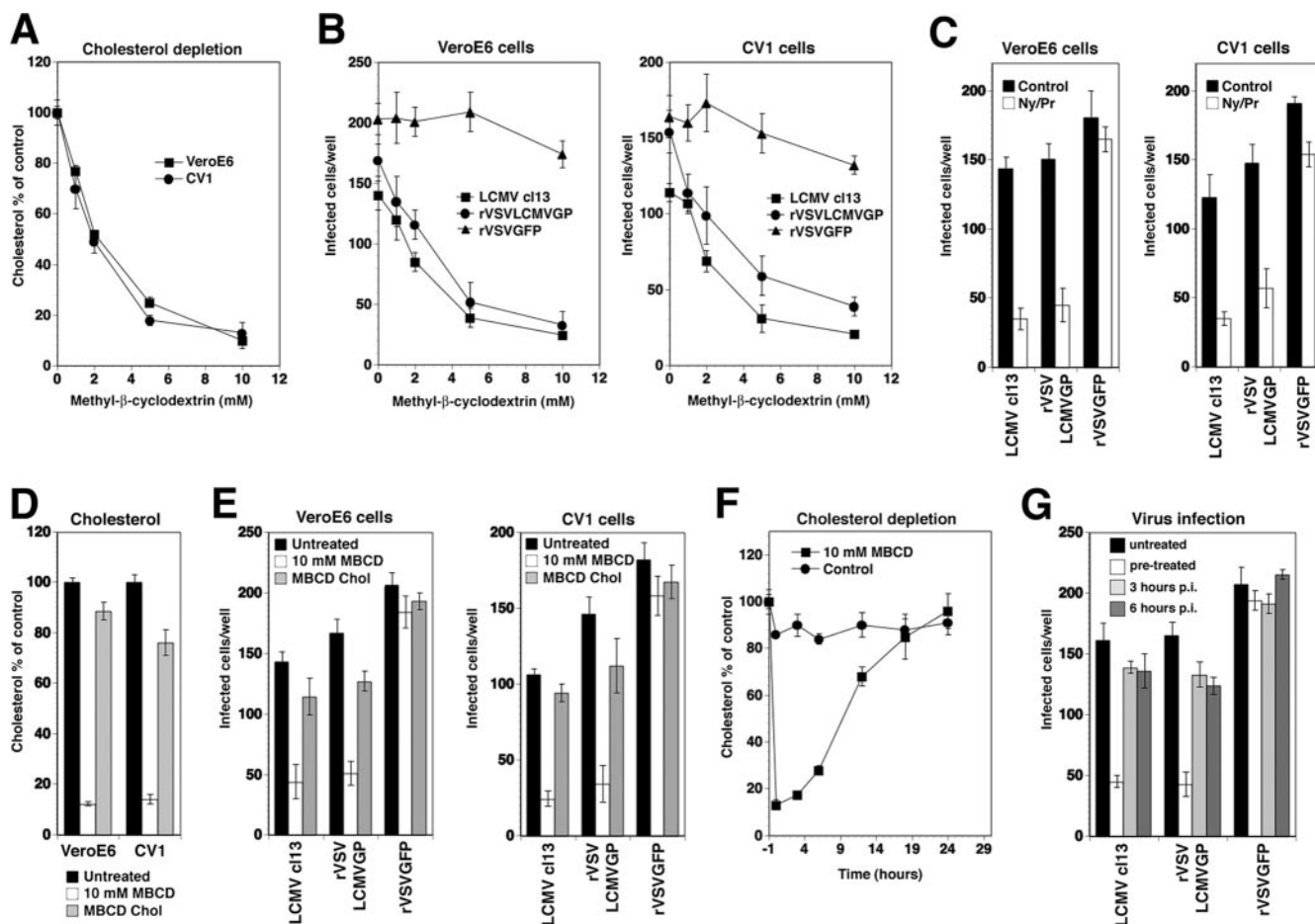
FIG. 2. Entry of LCMV depends on membrane cholesterol. (A) Depletion of membrane cholesterol by MBCD. Monolayers of Vero E6 and CV1 cells were incubated with the indicated concentrations of MBCD for 1 h, and the total amount of cholesterol was determined in a colorimetric assay. Data are triplicates expressed as percentages of values for the untreated control (means ± standard deviations). (B) Cholesterol depletion reduces infection with LCMV and rVSV-LCMV GP. Vero E6 and CV1 cells were treated with the concentrations of MBCD indicated for panel A and infected with 200 PFU each of LCMV cl-13, rVSV-LCMV GP, and rVSV-GFP. The level of infection was determined by immunofluorescence assay (values are means ± standard deviations; $n = 3$). (C) Reduction of LCMV and rVSV-LCMV GP infection after sequestration of membrane cholesterol. Vero E6 and CV1 cells were cultured in the presence of nystatin/progesterone (Ny/Pr) or control medium (control) for 16 h and then infected with 200 PFU each of LCMV cl-13, rVSV-LCMV GP, and rVSV-GFP in the presence of drugs. Infection was assessed as described for panel B (values are means ± standard deviations; $n = 3$). (D) Replenishment of cholesterol. Vero E6 and CV1 cells were left untreated or were treated with 10 mM MBCD, followed by either 1 h in serum-free medium or 1 h of incubation with cholesterol-loaded MBCD (MBCD Chol). Total cellular cholesterol was determined as described for panel A (values are means ± standard deviations; $n = 3$). (E) Cholesterol replenishment reverses the inhibition of infection. Cells left untreated, depleted with 10 mM MCBD, and replenished with MBCD-loaded cholesterol as described for panel D were infected with LCMV cl-13, rVSV-LCMV GP, and rVSV-GFP, and infection was determined as described for panel B (values are means ± standard deviations; $n = 3$). (F) Kinetics of cholesterol depletion by MBCD. Vero E6 cells were left untreated or were treated with 10 mM MBCD for 1 h and cultured in complete medium for up to 24 h. Total cholesterol was determined at the indicated time points as described for panel A (values are means ± standard deviations; $n = 3$). (G) Cholesterol depletion affects an early step of LCMV infection. Vero E6 cells were either left untreated, treated with 10 mM MBCD 1 h prior to infection (pretreated), or treated at 3 or 6 h postinfection (p.i.) with 200 PFU each of LCMV cl-13, rVSV-LCMV GP, and rVSV-GFP. Infection was assessed after 16 h as described for panel B (values are means ± standard deviations; $n = 3$).

with the GPs of LCMV cl-13 (VSVΔG*-LCMV GP) and VSV (VSVΔG*-VSV GP). Vero E6 and CV1 cells were pretreated with MBCD and nystatin/progesterone as described above and then infected with VSV pseudotypes. Infection was determined after 16 h by fluorescence detection of GFP. Treatment of cells with MBCD (Fig. 3A) or nystatin/progesterone (Fig. 3B) reduced the level of the subsequent infection of VSV pseudotypes containing the GPs of LFV and LCMV but not VSV. Again, normal virus infection was restored after the replenishment of cholesterol (Fig. 3A). Taken together, our

data indicate that the cholesterol dependence of entry is conserved between the Old World arenaviruses LCMV and LFV.

LCMV binding to cellular α-DG is independent of membrane cholesterol. Membrane cholesterol may be involved in LCMV entry in several ways, including the association of the cellular receptor α-DG with cholesterol-rich membrane domains. Vero E6 and CV1 cells express a form of α-DG that shows high-affinity binding to LCMV cl-13 in virus overlay assays (Fig. 4A), and virus infection can be blocked with an anti-α-DG monoclonal antibody (Fig. 4B).
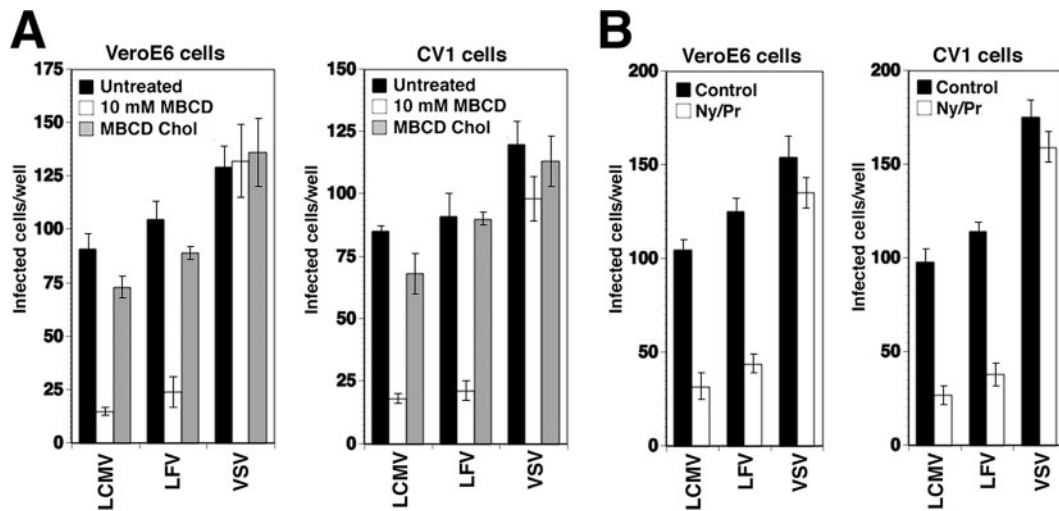
FIG. 3. LFV entry depends on membrane cholesterol. (A) Vero E6 and CV1 cells left untreated, depleted with 10 mM MBCD, or replenished with cholesterol as described for Fig. 2D were infected with 100 infectious units of VSV pseudotypes containing the GPs of LCMV cl-13 (LCMV), LFV, and VSV. Pseudotype infection was determined by the detection of the number of GFP-expressing cells per well (means ± standard deviations; $n = 3$). (B) Vero E6 and CV1 cells were treated with nystatin/progesterone as described for Fig. 2C and infected with 100 infectious units of the indicated VSV pseudotypes. Pseudotype infection was determined as described for panel A (means ± standard deviations; $n = 3$).

Membrane domains enriched in cholesterol and sphingolipids are operationally defined as lipid rafts based on their resistance to solubilization in cold Triton X-100 (68). Due to their lower buoyant density, such detergent-resistant membranes (DRMs) can be separated from the much larger fraction of detergent-soluble material in a sucrose gradient in flotation assays. To address the association of α-DG with DRMs, lysates of Vero E6 and CV1 cells were treated with 1% Triton X-100 at 4°C for 1 h and then subjected to a membrane flotation assay. The successful separation of DRMs was verified by the detection of the DRM marker protein caveolin-1. As shown in Fig. 4C, most α-DG in Vero E6 and CV1 cells was detected in detergent-soluble fractions at the bottom of the tube and not in caveolin-containing DRM fractions, indicating that α-DG is localized predominantly in non-raft membranes. In line with this observation, the extraction of membrane cholesterol with 10 mM MBCD had no detectable effect on the cell surface expression of α-DG as determined by flow cytometry (data not shown).

To examine the role of membrane cholesterol in virus attachment, a virus-cell binding assay was performed. To monitor virus binding to cells, we chose the transmembrane GP2 portion of LCMV GP as a marker. LCMV GP2 is anchored in the virion membrane and remains, under neutral pH and physiological salt concentrations, firmly attached to the receptor binding GP1 portion after binding to α-DG (37). For detection purposes, LCMV was labeled with biotin using the reagent NHS-X-biotin, which results in the efficient labeling of GP1 and GP2 without affecting virus infectivity (6, 38). Vero E6 and CV1 cells were treated with 10 mM MBCD for 1 h or left untreated. After cooling cells on ice to prevent virus internalization, biotinylated virus was added (100 PFU/cell) and incubated for increasing periods of time. After the removal of unbound virus, cells were lysed and LCMV GP2 was isolated by IP using MAb 83.6 to LCMV GP2 immobilized on Sepharose 4B (for details, see Materials and Methods). Immuno-

complexes were separated by SDS-PAGE, and biotinylated GP2 was detected with streptavidin-HRP by Western blotting. As indicated by the data displayed in Fig. 4D and E, virus binding was not affected by cholesterol depletion and occurred rapidly, with half-maximal binding after <10 min.

LCMV internalization depends on membrane cholesterol. Since the initial attachment of the virus to the cell occurred in non-raft membranes and was independent of cholesterol, we addressed the role of cholesterol in subsequent virus internalization. In order to differentiate between virus binding to the cell surface and uptake, we used a well-established internalization assay for the study of endocytosis of macromolecular ligands (64, 79) and viruses (54). For this purpose, virus was labeled with the reagent NHS-SS-biotin, resulting in a biotin label that is cleavable by reducing agents. In virus bound to the cell surface, and thus exposed to the extracellular space, the biotin label can be cleaved efficiently with the potent, membrane-impermeable reducing agent TCEP. However, once internalized, the biotin-labeled virus is protected from TCEP and retains its biotin group after treatment of cells with the reducing agent. This allows a clear distinction between virus particles bound to the cell surface and virus present in intracellular compartments. The labeling of purified LCMV by NHS-SS-biotin resulted in efficient biotinylation of LCMV GP2, and treatment with TCEP cleaved >95% of the biotin label (data not shown).

To monitor virus internalization, NHS-SS-biotin-labeled virus was bound to cells at 4°C for 1 h, unbound virus was removed, and cells were incubated at 37°C. After the indicated time points, cells were quickly chilled on ice to stop membrane movements and were treated with TCEP or reaction buffer only. After the quenching of residual TCEP, cells were lysed, LCMV GP2 was isolated by IP, and biotinylated GP2 was detected with Western blotting under nonreducing conditions. In control samples, similar amounts of cell-associated biotinylated GP2 were detected over time, indicating little disso-
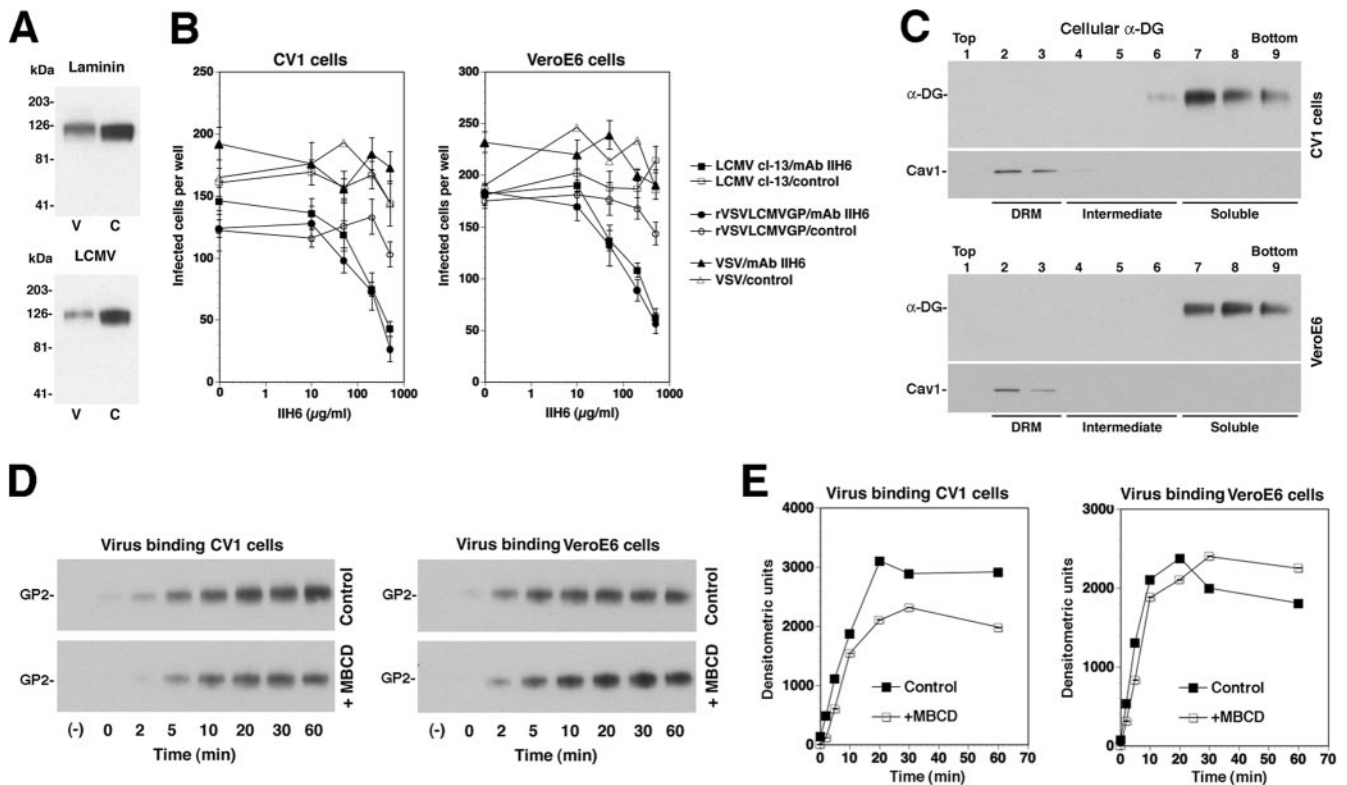
FIG. 4. Initial virus binding to α-DG occurs in non-raft membranes. (A) CV1 (C) and Vero E6 (V) cells express α-DG with high-affinity binding to LCMV and laminin. α-DG was isolated from CV1 and Vero E6 cells by wheat germ agglutinin lectin affinity purification. Binding to laminin was assessed by a laminin overlay assay using 10 μg/ml mouse laminin-1 and a polyclonal anti-laminin antibody, along with ECL for detection. For the virus overlay protein binding assay, blots were probed with 10^7 PFU/ml purified LCMV cl-13. Bound virus was detected with MAb 83.6, an HRP-conjugated secondary antibody, and ECL. (B) Blocking of LCMV cl-13 infection in CV1 and Vero E6 cells with MAb IIH6 (anti-α-DG). Cells were blocked with the indicated concentrations of MAb IIH6 or an unrelated mouse IgM (control) for 2 h at 4°C. LCMV cl-13, rVSV-LCMV GP, or VSV (200 PFU of each) was added for 45 min, and infection was assessed by the detection of LCMV NP and VSV NP with specific MAbs and fluorescein isothiocyanate-conjugated secondary antibodies in immunofluorescence. Data points represent values for triplicate samples ± standard deviations. (C) α-DG partitions into non-raft membranes. CV1 and Vero E6 cells were extracted with 1% Triton X-100 at 4°C, and samples were floated in a linear sucrose gradient. α-DG and the DRM marker caveolin-1 (Cav1) were detected in individual fractions by Western blotting with specific antibodies. DRMs, intermediate fractions, and detergent-soluble fractions are indicated. (D) Binding of LCMV to cells does not depend on membrane cholesterol. CV1 and Vero E6 cells either were treated with 10 mM MBCD for 1 h (+MBCD) or left untreated (control). Cells then were chilled on ice and incubated with purified biotinylated LCMV (100 PFU/cell). After the indicated times, unbound virus was removed, cells were washed and lysed, and LCMV GP2 was isolated by IP. Biotinylated GP2 in IPs was detected by Western blotting using HRP-conjugated streptavidin. (E) Quantification of results shown in panel D. X-ray films were analyzed by densitometry.

ciation of bound virus (Fig. 5A). This is consistent with previous observations that LCMV cl-13 binds to its cellular receptor α-DG with high affinity in a virtually irreversible manner (37). In samples treated with TCEP, biotinylated GP2 became detectable after circa 20 min, with an increase over the next 30 to 90 min (Fig. 5A, B). Compared to the total amount of cell-associated biotinylated GP2 detected in untreated samples, the amount of biotinylated GP2 protected from TCEP was small (circa 15% of cell-associated virus), possibly due to inefficient uptake of labeled virus and/or only partial protection against the reducing agent.

To address the role of membrane cholesterol in virus uptake, cells were pretreated with 10 mM MBCD for 1 h. Cells were chilled on ice, and biotinylated virus was added for 1 h in the cold. Cells then were shifted to 37°C for 1 h to allow internalization and then either treated with TCEP or left untreated. We detected no significant change in total cell-associated GP2 in cells treated with MBCD but a marked reduction in inter-

nalized GP2 (Fig. 5C), indicating that virus internalization depends on membrane cholesterol.

Entry of LCMV is independent of clathrin and caveolin and does not require dynamin. The best characterized among the clathrin-independent, cholesterol-dependent endocytotic pathways involved in viral entry are caveolar pathways (31, 42). Since many cell types infected by Old World arenaviruses are rich in caveolae, we addressed the role of caveolae in arenavirus entry. To this end, we utilized the recently developed DN caveolin-1 mutant cav-1Y14F (14), which is unable to undergo phosphorylation at tyrosine residue Y14 and is deficient in some caveolin functions, including coxsackievirus entry. Cholesterol-dependent endocytotic pathways also frequently involve the recruitment of the GTPase dynamin, which is crucial for the final stage of vesicle scission. The DN mutant K44A of dynamin I, Dyn1K44A, has been shown to inhibit the function of both endogenous dynamin I and dynamin II and to block clathrin-mediated and caveolar endocytosis (15, 49). In addi-
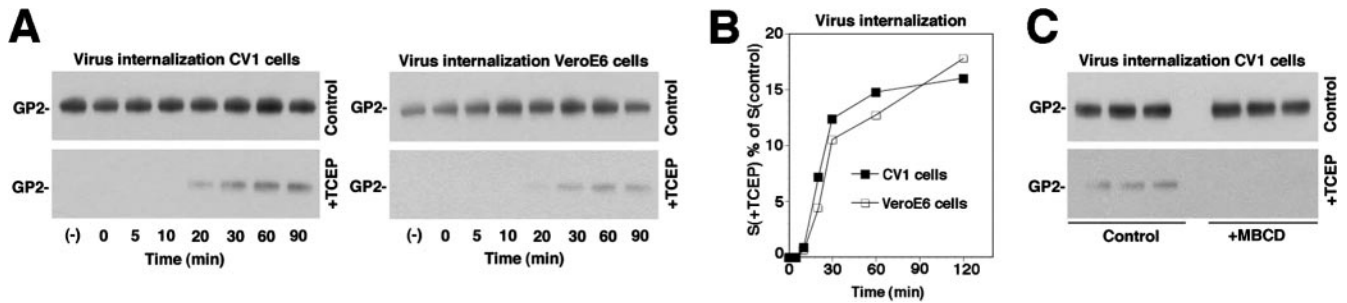
FIG. 5. LCMV internalization depends on membrane cholesterol. (A) Internalization of LCMV. CV1 and Vero E6 cells were incubated with LCMV labeled with NHS-SS-biotin (100 PFU/cell) for 1 h on ice, unbound virus was removed, and cells were shifted to 37°C. After the indicated time periods, cells were chilled on ice and treated either with TCEP (+TCEP) or reaction buffer only (control). After the removal of TCEP, cells were lysed, LCMV GP2 was isolated by IP, and biotinylated GP2 was detected by nonreducing Western blotting with HRP-conjugated streptavidin. (B) Quantification of the results shown in panel A, with the signals for GP2 in untreated (control) cells set as 100%. For each time point, the ratio of the signal obtained with TCEP-treated cells, S(+TCEP), divided by the signal from control cells, S(control), was calculated in percentages and plotted against the incubation time. (C) LCMV internalization depends on membrane cholesterol. Triplicate samples of CV1 cells were treated for 1 h at 37°C with either 10 mM MBCD (+MBCD) or control medium (control). After chilling the cells on ice, NHS-SS-biotin-labeled LCMV was added for 1 h in the cold. Cells then were shifted to 37°C for 1 h, and an LCMV internalization assay was performed as described for panel A.

tion, we used the K44A mutant of dynamin II (76). To exclude the involvement of clathrin-mediated endocytosis, we included a DN mutant of the clathrin coat-associated protein Eps15, Eps15Δ95/295, lacking the second and third of the three EH domains of Eps15. The overexpression of Eps15Δ95/295 results in a DN protein that specifically interferes with clathrin-coated pit assembly (4) without affecting clathrin-independent endocytotic pathways (48). To distinguish the specific effect of the DN mutants from changes caused by the overexpression of the transgenes, we directly compared GFP-tagged versions of the wild-type forms to those of the DN mutants, using the GFP label for the assessment of transgene expression levels.

CV1 cells were transfected with GFP-tagged versions of the wild-type forms and the DN mutants of caveolin-1, dynamin I, dynamin II, and Eps15. Twenty-four hours posttransfection, cells were infected with LCMV cl-13. As a control virus to test the activity of the DN mutants, we included the clade B New World arenavirus Junin virus (vaccine strain Candid 1), which uses transferrin receptor 1 as a cellular receptor (58) and enters cells via clathrin-mediated endocytosis (43). After 16 h of infection, cells were fixed and analyzed for infection by immunofluorescence staining for LCMV NP or Junin virus antigen. Specimens were examined by fluorescence microscopy, and cells that expressed similar levels of the GFP-tagged wild type and DN mutants were selected. The percentage of infection in transgene-expressing cells was determined by scoring cells expressing viral antigens. As shown in Fig. 6, the expression of the DN mutant Y14F of caveolin-1 had no effect on the infection of cells with either LCMV cl-13 or Junin virus. Interestingly, the expression of DN dynamin I, dynamin II, and Eps15 did not affect infection with LCMV cl-13 but caused a significant reduction in infection with Junin virus (Fig. 6). As expected, the DN mutants of dynamin I, dynamin II, and Eps15 also inhibited the uptake of transferrin (data not shown).

Since the caveolin-1 DN mutant used in our studies may block some functions of caveolin-1 but not others, we addressed the role of caveolae in LCMV entry using a complementary approach: the depletion of caveolin-1 by RNA interference. Out of the three caveolin isoforms present in mammals, the formation of caveolae requires the expression of either caveolin-1 or caveolin-3, with the latter being restricted to muscle cells. Caveolin-2, although frequently coexpressed and associated with caveolin-1, cannot form caveolae alone (51). To address the role of caveolae in LCMV entry into CV1 epithelial cells, we depleted caveolin-1 by using a pool of four synthetic siRNAs targeting the ORF of the human homologue. Due to the high sequence conservation between caveolin-1 from humans and that from the North African green monkey (*C. aethiops*), from which CV1 cells are derived, three out of four human caveolin siRNAs perfectly matched both sequences, and the fourth siRNA had only a single base mismatch (for details, see Materials and Methods). The pool of caveolin-1-specific siRNAs and control siRNA was transfected into CV1 cells as described previously (63). Cells were lysed after 48 h and caveolin-1 was detected by Western blotting, using α-tubulin for normalization. Transfection with caveolin-1 siRNAs resulted consistently in a >80% reduction in caveolin expression compared to that of control siRNA (Fig. 7A, B). CV1 cells transfected with caveolin-1 or control siRNAs then were infected with LCMV cl-13 at a low MOI (0.01). Junin virus Candid 1, the entry of which is independent of caveolae (43), again served as a negative control. As a positive control, we used SV40, which enters CV1 cells by caveolar endocytosis (53, 54).

Infection of LCMV cl-13 and Junin virus Candid 1 was assessed after 16 h by immunofluorescence as described above. SV40 infection was determined by immunostaining for the SV40 T antigen (53, 54). As shown in Fig. 7C, the marked depletion of caveolin-1 in cells treated with the specific siRNA had no significant effect on infection with LCMV cl-13 and Junin virus, making a critical role for caveolae in infection unlikely. In contrast, treatment with caveolin-1 siRNA resulted in a moderate (circa 40%) but consistent and specific reduction of infection with SV40, as reported previously (52), indicating significant impairment of caveolar endocytosis by the extent of caveolin-1 depletion achieved.

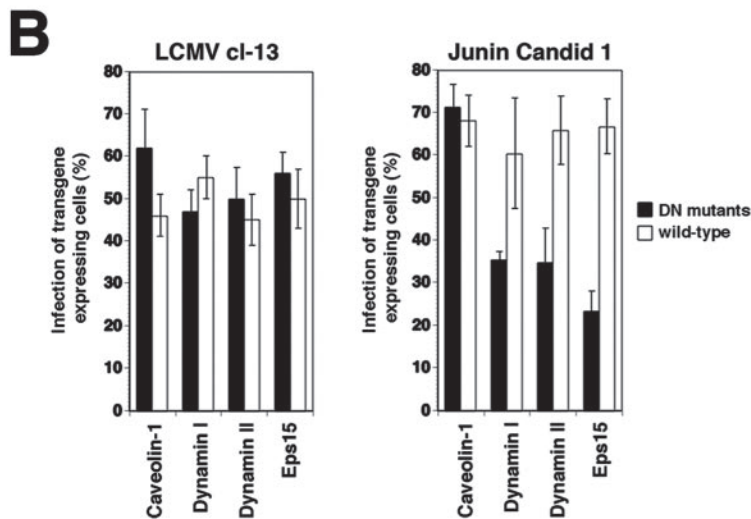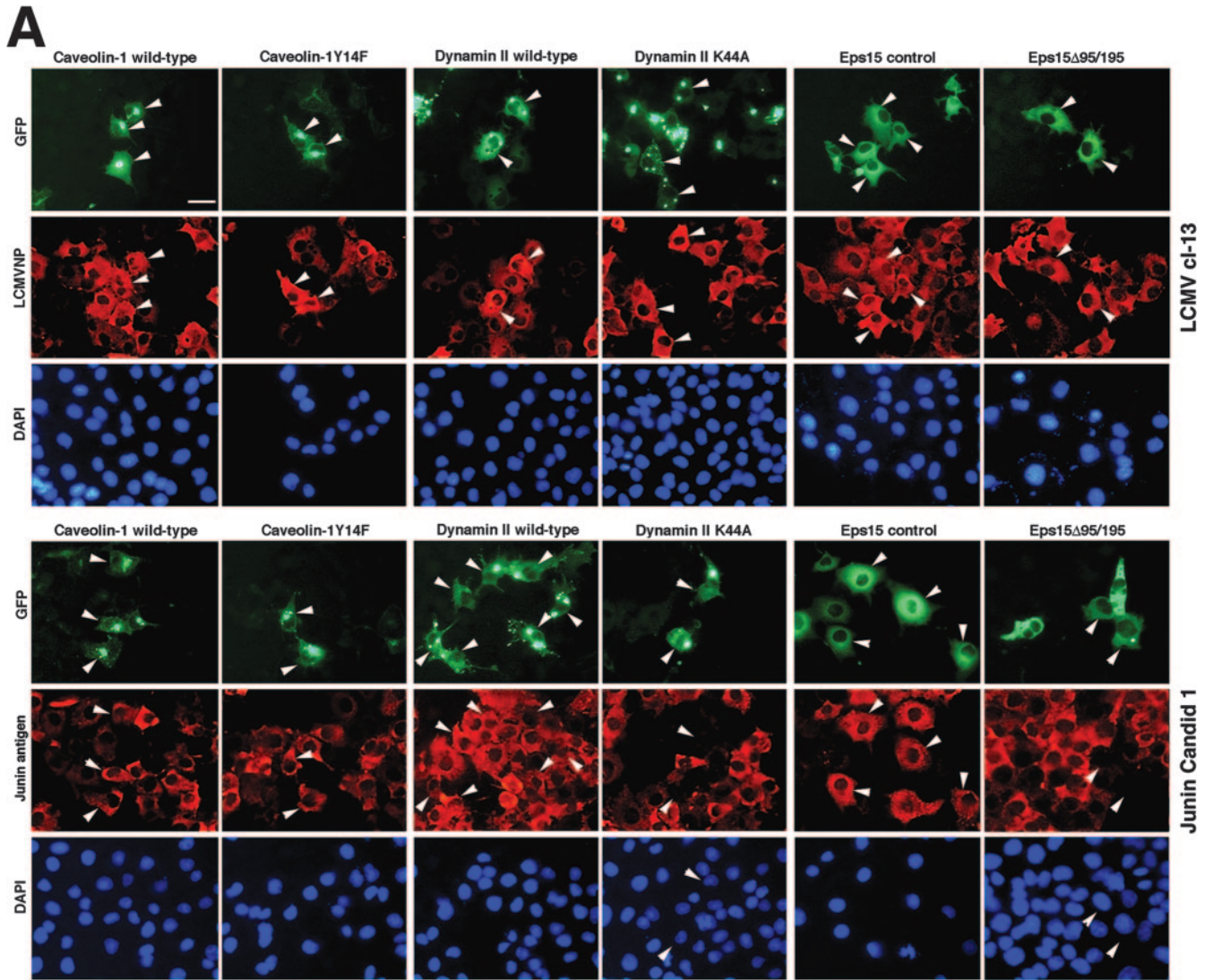To further confirm the ability of LCMV to enter cells inde-

FIG. 6. Infection with LCMV occurs independently of caveolin-1, dynamin, and Esp15, while infection with Junin virus requires clathrin and dynamin. (A) CV1 cells were transfected with the GFP-tagged wild type and DN mutants of caveolin-1, dynamin I (not shown), dynamin II, and Eps15. Twenty hours posttransfection, cells were infected with either LCMV cl-13 or Junin virus Candid 1 at an MOI of 5. After 16 h, cells were fixed and infection was assessed by immunofluorescence detection of LCMV NP or Junin virus antigen using a rhodamine red-X-conjugated secondary antibody (red). Cell nuclei were counterstained with DAPI (bar, 20 μm). (B) For quantification, 100 cells with similar levels of transgene expression, as assessed by the intensity of their GFP signals, and cells positive for viral antigen were screened (means ± standard deviations; n = 3). Note that cells with high expression levels of Eps15Δ95/195 show signs of cytopathic effect and were excluded from the analysis.
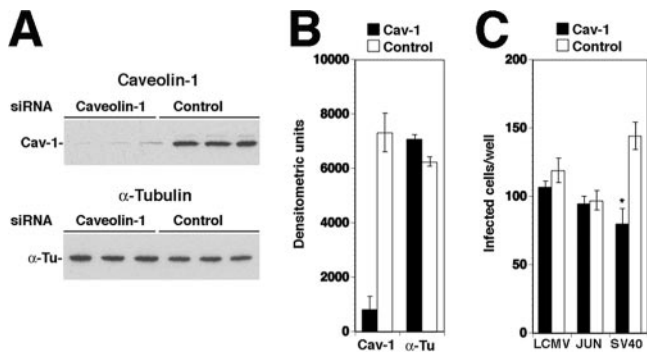
FIG. 7. Depletion of caveolin-1 does not affect infection with LCMV. (A) Depletion of caveolin-1 from CV1 cells by siRNA. Triplicate samples of CV1 cells were transfected either with a pool of siRNA targeting caveolin (50 nM per siRNA, 200 nM total concentration) or with control siRNA (200 nM). After 48 h, cells were lysed and caveolin-1 (Cav-1) and α-tubulin (α-Tu) were detected by Western blotting. (B) Quantification of results shown in panel A using densitometry (means ± standard deviations; $n = 3$). (C) Caveolin depletion does not affect infection with LCMV cl-13 and Junin virus Candid 1. Cells transfected with siRNA to either caveolin (Cav-1) or control siRNAs (Control) as described for panel A were infected with LCMV cl-13, Junin virus Candid 1, or SV40 (200 PFU per well, corresponding to an MOI of 0.01). Cells were fixed after 16 h. Infections with LCMV cl-13 and Junin virus Candid 1 were assessed as described for Fig. 6A. For the detection of SV40 infection, cells were stained with an antibody to the SV40 T antigen and a fluorescence-conjugated secondary antibody. Cells positive for viral antigen were scored (values are means ± standard deviations; $n = 3$). Asterisks indicate significant Student's t test values ($P < 0.01$).

pendently of caveolae, we looked at the infection of the human hepatocyte line Huh7, which is naturally deficient in caveolin-1 and caveolin-2 and thus lacks caveolae (16). Despite being deficient in caveolin-1 (Fig. 8A), Huh7 cells turned out to be

highly susceptible to infection with VSV pseudotypes of LCMV, LFV, and VSV (Fig. 8B). As in the case of caveolin-1-positive Vero E6 and CV1 cells, infection with VSV pseudotypes of LCMV and LFV, but not VSV, critically depended on membrane cholesterol (Fig. 8C). Although the specific mechanism of viral entry may differ among cell types, our data show that LCMV can efficiently infect cells naturally devoid of caveolae.

Neither structural integrity nor dynamics of the actin cytoskeleton are required for LCMV infection. Initial studies documented that the disruption of actin microfilaments by cytochalasin D did not reduce LCMV infection (7), indicating that the structural integrity of actin fibers is not required. To address a possible role of actin dynamics in LCMV entry, we compared the effects of cytochalasin D to those of latrunculin A, an actin monomer-sequestering drug, and jasplakinolide, an actin polymer-stabilizing drug that blocks the dynamics of actin filaments. When added to CV1 or Vero E6 cells for 30 min, cytochalasin D, latrunculin A, and jasplakinolide induced the expected changes in the cellular actin cytoskeleton (Fig. 9A) but had no effect on LCMV infection (Fig. 9B), indicating that neither the structural integrity nor the dynamics of the actin cytoskeleton are required for LCMV entry and early replication.

DISCUSSION

We investigated the entry of the prototypic Old World arenavirus LCMV and make the following points. The initial attachment of LCMV to its cellular receptor α-DG occurs independently of cholesterol, followed by internalization by a cholesterol-dependent mechanism. The endocytotic pathway involved in LCMV entry is independent of clathrin and caveolin and does not require dynamin or actin, features that are
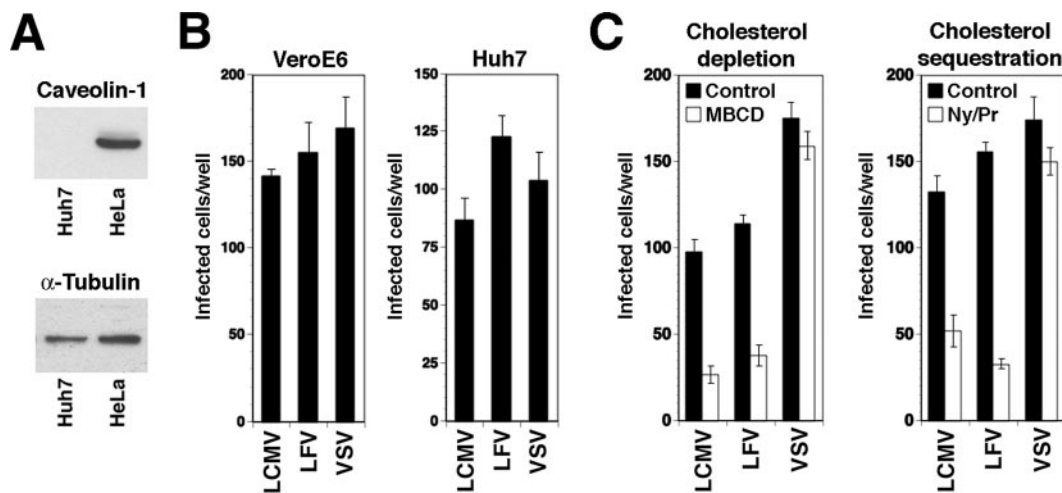

FIG. 8. Infection of caveolin-1-deficient Huh7 cells with pseudotypes of LCMV and LFV. (A) Detection of caveolin-1 in total lysates of Huh7 and HeLa cells by Western blotting. The loading control was the detection of α-tubulin. (B) Infection of Vero E6 and Huh7 cells with VSV pseudotypes of LFV and LCMV. Cells were infected with 200 infectious units of the indicated VSV-based pseudotypes, and the infection status was determined after 24 h by the detection of the GFP reporter. Doublets of infected cells were counted as one infectious event (means ± standard deviations; $n = 3$). (C) Infection of Huh7 cells with LCMV and LFV pseudotypes is dependent on membrane cholesterol. Huh7 cells either were treated with 10 mM MBCD for 1 h (cholesterol depletion) or were incubated for 16 h with nystatin/progesterone (cholesterol sequestration) and infected with 200 infectious units of the indicated VSV pseudotypes. Infection was assessed by the detection of the GFP reporter as described for panel B (values are means ± standard deviations; $n = 3$).
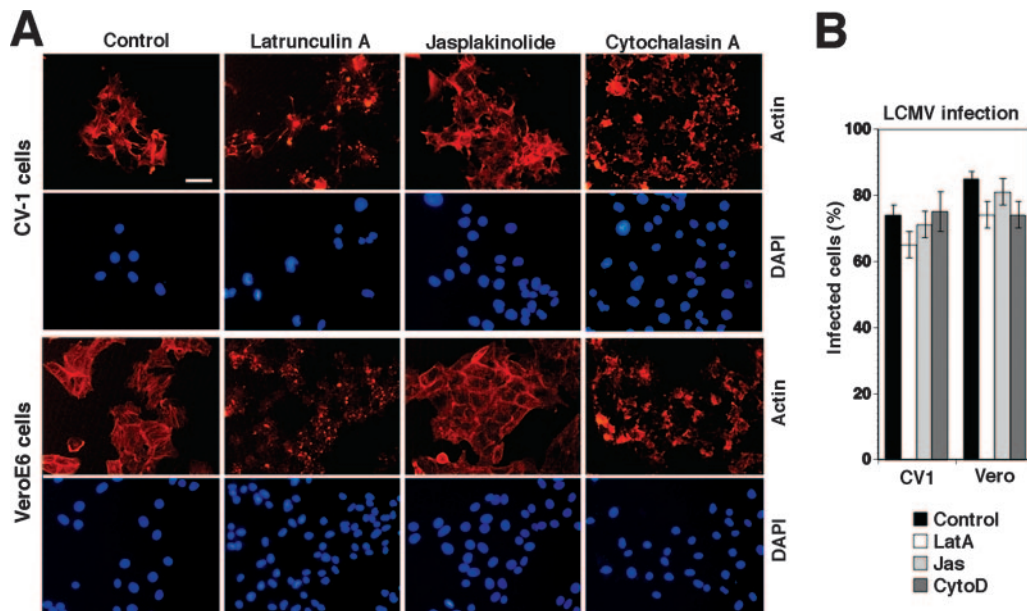
FIG. 9. Neither structural integrity nor dynamics of the actin cytoskeleton are needed for LCMV infection. (A) CV1 and Vero cells were treated with 1 μM latrunculin A (LatA), 500 nM jasplakinolide (Jas), and 25 μg/ml cytochalasin D (CytoD) for 1 h or were left untreated (control). Cells then were fixed, and actin filaments were visualized with phalloidin conjugated to rhodamine. Cell nuclei were counterstained with DAPI (bar, 20 μm). (B) Quantitative determination of LCMV infection in cells treated as described for panel A by intracellular staining for LCMV NP using MAb 113 combined with a phycoerythrin-conjugated secondary antibody and flow cytometry. Data were acquired in a FACSCalibur flow cytometer and analyzed using FloJo software, and NP-expressing cells were scored (values are means ± standard deviations; $n = 3$).

strikingly different from those of the pathway used by the New World arenavirus Junin virus and other enveloped viruses.

Initial studies revealed that upon binding to its cellular receptor, LCMV enters cells via noncoated vesicles, followed by pH-dependent membrane fusion in an endosomal compartment (7). More recent studies indicated a role of membrane cholesterol in infection (66), suggesting that a cholesterol-dependent endocytotic pathway was involved in virus entry.

To specifically address the role of membrane cholesterol for LCMV entry, a recombinant VSV containing the GP of LCMV cl-13 (rVSV-LCMV GP) was generated. This approach was based on the fact that infection by and replication of VSV is not dependent on cholesterol (66) and that the arenavirus GP is necessary and sufficient for viral entry. Employing well-characterized drugs that either deplete or sequester membrane cholesterol, it was revealed that cholesterol is indeed required for LCMV entry but is not needed for later steps in infection. A similar requirement for membrane cholesterol was found for the entry of LFV, another member of the Old World arenavirus family.

Since the entry of Old World arenaviruses is likely a multistep process, membrane cholesterol may be involved in different ways. First, we addressed a possible role of membrane cholesterol for virus-receptor binding. An examination of the partition of α-DG into DRMs by flotation assay provided no evidence for an association of α-DG with cholesterol-rich lipid raft domains. Consistent with the location of the receptor in non-raft membranes, virus attachment was not affected by cholesterol depletion. In contrast, subsequent internalization of the virus was sensitive to cholesterol depletion, implicating a cholesterol-dependent pathway of endocytosis.

Although our data clearly implicated membrane cholesterol in Old World arenavirus entry, the cholesterol dependence of endocytosis was defined operationally as the sensitivity to cholesterol extraction and sequestration. Experimental conditions were optimized to avoid a general perturbation of membrane properties, as illustrated by the unaffected entry of VSV, which uses clathrin-mediated endocytosis (73). However, our data still could cover a wide range of endocytotic pathways and therefore by no means implicate a specific mechanism of entry. For further characterization of the endocytotic pathway used by LCMV, we utilized a set of well-characterized DN mutants of caveolin-1, dynamin I, dynamin II, and the clathrin coat-associated protein Eps15. As a control, we used the clade B New World arenavirus Junin virus, which uses clathrin-mediated endocytosis for entry (43). While the overexpression of DN dynamin I, dynamin II, and Eps15 significantly blocked infection with Junin virus, the DN mutants had no effect on LCMV infection. This is consistent with earlier immune-electron microscopy studies that reported the binding of LCMV to cells outside of coated pits and the detection of LCMV predominantly in noncoated vesicles (7) (Fig. 2). The striking difference in the roles of clathrin and dynamin in the entry of the Old World arenavirus LCMV and the New World virus Junin may be a consequence of the use of distinct cellular receptors by these viruses. While LCMV cl-13 uses α-DG, Junin virus and the other pathogenic clade B New World arenaviruses Guanarito, Machupo, and Sabia use human transferrin receptor 1 (58), a classical cargo receptor internalized by clathrin-mediated endocytosis (13).

The lack of inhibition of LCMV infection by either overexpression of the caveolin-1 DN mutant Y14F or depletion of caveolin-1 by siRNA indicates a noncaveolar mechanism of entry. This is consistent with the efficient infection of caveolin-

deficient Huh7 cells with LCMV pseudotypes demonstrated in this study and the fact that caveolae are rare or absent from some cell types infected by LCMV in vivo and in vitro, including hepatocytes and neuronal cells (51).

Initial studies on the role of the actin cytoskeleton for LCMV infection revealed that the disruption of actin microfilaments by cytochalasin D has no effect on virus infection (7). Extending the findings of these studies, we confirm that neither the structural integrity nor the dynamics of actin fibers are required for LCMV entry and early infection. This rules out a mechanism of viral entry involving macropinocytosis, which critically depends on actin dynamics (13, 20, 30, 41).

In sum, our data indicate that the endocytotic pathway used by LCMV is cholesterol dependent, clathrin independent, and caveolin independent, and it is at least not blocked by DN mutants of dynamin that inhibit clathrin- and caveolin-dependent pathways. The pathway involved in LCMV entry therefore appears to be different from the clathrin-dependent endocytosis pathway used by other enveloped viruses such as Semliki Forest virus (67), VSV (73), and Junin virus (43), as well as the caveolar pathways used by nonenveloped viruses like SV40 (53, 54, 71), picornaviruses (14, 57), and polyomavirus (28). Interestingly, the characteristics of the endocytotic pathway used by LCMV uncovered here resemble in some respects those of a recently discovered cholesterol-dependent, clathrin-, caveolin-, and dynamin-independent pathway used by SV40 in cells devoid of caveolae (16, 33, 34). However, in contrast to SV40, which is targeted to pH-neutral compartments like the endoplasmic reticulum (16), the pH profile of LCMV membrane fusion requires the delivery of the virus to late endosomes. Since the cellular factors involved in LCMV entry are largely unknown so far, a possible relationship between the two pathways remains speculative at this point. We currently are aiming at the identification of the host cell factors required for LCMV entry, which should provide novel insights into virus-host cell interaction and may illuminate novel drug targets for the development of antiarenaviral strategies.

ACKNOWLEDGMENTS

REFERENCES

1. Ahmed, R., A. Salmi, L. D. Butler, J. M. Chiller, and M. B. Oldstone. 1984. Selection of genetic variants of lymphocytic choriomeningitis virus in spleens of persistently infected mice. Role in suppression of cytotoxic T lymphocyte response and viral persistence. J. Exp. Med. 160:521–540.
2. Barresi, R., and K. P. Campbell. 2006. Dystroglycan: from biosynthesis to pathogenesis of human disease. J. Cell Sci. 119:199–207.
3. Bender, F. C., J. C. Whitbeck, M. Ponce de Leon, H. Lou, R. J. Eisenberg, and G. H. Cohen. 2003. Specific association of glycoprotein B with lipid rafts during herpes simplex virus entry. J. Virol. 77:9542–9552.
4. Benmerah, A., M. Bayrou, N. Cerf-Bensussan, and A. Dautry-Varsat. 1999. Inhibition of clathrin-coated pit assembly by an Eps15 mutant. J. Cell Sci. 112:1303–1311.
5. Benmerah, A., C. Lamaze, B. Begue, S. L. Schmid, A. Dautry-Varsat, and N. Cerf-Bensussan. 1998. AP-2/Eps15 interaction is required for receptor-mediated endocytosis. J. Cell Biol. 140:1055–1062.
6. Borrow, P., and M. B. Oldstone. 1992. Characterization of lymphocytic choriomeningitis virus-binding protein(s): a candidate cellular receptor for the virus. J. Virol. 66:7270–7281.
7. Borrow, P., and M. B. Oldstone. 1994. Mechanism of lymphocytic choriomeningitis virus entry into cells. Virology 198:1–9.
8. Buchmeier, M. J., J. C. de la Torre, and C. J. Peters. 2007. Arenaviridae: the viruses and their replication, p. 1791–1828. In D. L. Knipe and P. M. Howley (ed.), Fields virology, 5th ed. Lippincott-Raven, Philadelphia, PA.
9. Buchmeier, M. J., H. A. Lewicki, O. Tomori, and M. B. Oldstone. 1981. Monoclonal antibodies to lymphocytic choriomeningitis and pichinde viruses: generation, characterization, and cross-reactivity with other arenaviruses. Virology 113:73–85.
10. Cao, W., M. D. Henry, P. Borrow, H. Yamada, J. H. Elder, E. V. Ravkov, S. T. Nichol, R. W. Compans, K. P. Campbell, and M. B. Oldstone. 1998. Identification of α-dystroglycan as a receptor for lymphocytic choriomeningitis virus and Lassa fever virus. Science 282:2079–2081.
11. Castilla, V., S. E. Mersich, N. A. Candurra, and E. B. Damonte. 1994. The entry of Junin virus into Vero cells. Arch. Virol. 136:363–374.
12. Choi, K. S., H. Aizaki, and M. M. Lai. 2005. Murine coronavirus requires lipid rafts for virus entry and cell-cell fusion but not for virus release. J. Virol. 79:9862–9871.
13. Conner, S. D., and S. L. Schmid. 2003. Regulated portals of entry into the cell. Nature 422:37–44.
14. Coyne, C. B., and J. M. Bergelson. 2006. Virus-induced Abl and Fyn kinase signals permit coxsackievirus entry through epithelial tight junctions. Cell 124:119–131.
15. Damke, H., T. Baba, D. E. Warnock, and S. L. Schmid. 1994. Induction of mutant dynamin specifically blocks endocytic coated vesicle formation. J. Cell Biol. 127:915–934.
16. Damm, E. M., L. Pelkmans, J. Kartenbeck, A. Mezzacasa, T. Kurzchalia, and A. Helenius. 2005. Clathrin- and caveolin-1-independent endocytosis: entry of simian virus 40 into cells devoid of caveolae. J. Cell Biol. 168:477–488.
17. Danthi, P., and M. Chow. 2004. Cholesterol removal by methyl-β-cyclodextrin inhibits poliovirus entry. J. Virol. 78:33–41.
18. Di Simone, C., and M. J. Buchmeier. 1995. Kinetics and pH dependence of acid-induced structural changes in the lymphocytic choriomeningitis virus glycoprotein complex. Virology 209:3–9.
19. Di Simone, C., M. A. Zandonatti, and M. J. Buchmeier. 1994. Acidic pH triggers LCMV membrane fusion activity and conformational change in the glycoprotein spike. Virology 198:455–465.
20. Döhner, K., and B. Sodeik. 2005. The role of the cytoskeleton during viral infection. Curr. Top. Microbiol. Immunol. 285:67–108.
21. Dutko, F. J., and M. B. Oldstone. 1983. Genomic and biological variation among commonly used lymphocytic choriomeningitis virus strains. J. Gen. Virol. 64:1689–1698.
22. Ervasti, J. M., and K. P. Campbell. 1993. A role for the dystrophin-glycoprotein complex as a transmembrane linker between laminin and actin. J. Cell Biol. 122:809–823.
23. Eschli, B., K. Quirin, A. Wepf, J. Weber, R. Zinkernagel, and H. Hengartner. 2006. Identification of an N-terminal trimeric coiled-coil core within arenavirus glycoprotein 2 permits assignment to class I viral fusion proteins. J. Virol. 80:5897–5907.
24. Fischer, S. A., M. B. Graham, M. J. Kuehnert, C. N. Kotton, A. Srinivasan, F. M. Marty, J. A. Comer, J. Guarner, C. D. Paddock, D. L. DeMeo, W. J. Shieh, B. R. Erickson, U. Bandy, A. DeMaria, Jr., J. P. Davis, F. L. Delmonico, B. Pavlin, A. Likos, M. J. Vincent, T. K. Sealy, C. S. Goldsmith, D. B. Jernigan, P. E. Rollin, M. M. Packard, M. Patel, C. Rowland, R. F. Helfand, S. T. Nichol, J. A. Fishman, T. Ksiazek, and S. R. Zaki. 2006. Transmission of lymphocytic choriomeningitis virus by organ transplantation. N. Engl. J. Med. 354:2235–2249.
25. Fuerst, T. R., E. G. Niles, F. W. Studier, and B. Moss. 1986. Eukaryotic transient-expression system based on recombinant vaccinia virus that synthesizes bacteriophage T7 RNA polymerase. Proc. Natl. Acad. Sci. USA 83:8122–8126.
26. Gallaher, W. R., C. DiSimone, and M. J. Buchmeier. 2001. The viral transmembrane superfamily: possible divergence of arenavirus and filovirus glycoproteins from a common RNA virus ancestor. BMC Microbiol. 1:1.
27. Geisbert, T. W., and P. B. Jahrling. 2004. Exotic emerging viral diseases: progress and challenges. Nat. Med. 10:S110—S121.
28. Gilbert, J., and T. Benjamin. 2004. Uptake pathway of polyomavirus via ganglioside GD1a. J. Virol. 78:12259–12267.
29. Gosselin-Grenet, A. S., G. Mottet-Osman, and L. Roux. 2006. From assembly

to virus particle budding: pertinence of the detergent resistant membranes. Virology **344**:296–303.

30. **Greber, U. F., and M. Way.** 2006. A superhighway to virus infection. Cell **124**:741–754.

31. **Helenius, A.** 2007. Virus entry and uncoating, p. 99–118. *In* D. L. Knipe and P. M. Howley (ed.), Fields virology, 5th ed. Lippincott-Raven, Philadelphia, PA.

32. **Jamieson, D. J., A. P. Kourtis, M. Bell, and S. A. Rasmussen.** 2006. Lymphocytic choriomeningitis virus: an emerging obstetric pathogen? Am. J. Obstet. Gynecol. **194**:1532–1536.

33. **Kirkham, M., A. Fujita, R. Chadda, S. J. Nixon, T. V. Kurzchalia, D. K. Sharma, R. E. Pagano, J. F. Hancock, S. Mayor, and R. G. Parton.** 2005. Ultrastructural identification of uncoated caveolin-independent early endocytic vehicles. J. Cell Biol. **168**:465–476.

34. **Kirkham, M., and R. G. Parton.** 2005. Clathrin-independent endocytosis: new insights into caveolae and non-caveolar lipid raft carriers. Biochim. Biophys. Acta **1746**:349–363.

35. **Kunz, S., J. Rojek, M. Perez, C. Spiropoulou, and M. B. Oldstone.** 2005. Characterization of the interaction of Lassa fever virus with its cellular receptor α-dystroglycan. J. Virol. **79**:5979–5987.

36. **Kunz, S., J. Rojek, C. Spiropoulou, R. Barresi, K. P. Campbell, and M. B. Oldstone.** 2005. Posttranslational modification of α-dystroglycan, the cellular receptor for arenaviruses by the glycosyltransferase LARGE is critical for virus binding. J. Virol. **79**:14282–14296.

37. **Kunz, S., N. Sevilla, D. B. McGavern, K. P. Campbell, and M. B. Oldstone.** 2001. Molecular analysis of the interaction of LCMV with its cellular receptor α-dystroglycan. J. Cell Biol. **155**:301–310.

38. **Kunz, S., N. Sevilla, J. M. Rojek, and M. B. Oldstone.** 2004. Use of alternative receptors different than α-dystroglycan by selected isolates of lymphocytic choriomeningitis virus. Virology **325**:432–445.

39. **Kunz, S., U. Ziegler, B. Kunz, and P. Sonderegger.** 1996. Intracellular signaling is changed after clustering of the neural cell adhesion molecules axonin-1 and NgCAM during neurite fasciculation. J. Cell Biol. **135**:253–267.

40. **Lefrancois, L., and D. S. Lyles.** 1982. The interaction of antibody with the major surface glycoprotein of vesicular stomatitis virus. II. Monoclonal antibodies of nonneutralizing and cross-reactive epitopes of Indiana and New Jersey serotypes. Virology **121**:168–174.

41. **Marsh, M., and A. Helenius.** 1989. Virus entry into animal cells. Adv. Virus Res. **36**:107–151.

42. **Marsh, M., and A. Helenius.** 2006. Virus entry: open sesame. Cell **124**:729–740.

43. **Martinez, M. G., S. M. Cordo, and N. A. Candurra.** 2007. Characterization of Junin arenavirus cell entry. J. Gen. Virol. **88**:1776–1784.

44. **McCormick, J. B., and S. P. Fisher-Hoch.** 2002. Lassa fever. Curr. Top. Microbiol. Immunol. **262**:75–109.

45. **Michele, D. E., R. Barresi, M. Kanagawa, F. Saito, R. D. Cohn, J. S. Satz, J. Dollar, I. Nishino, R. I. Kelley, H. Somer, V. Straub, K. D. Mathews, S. A. Moore, and K. P. Campbell.** 2002. Post-translational disruption of dystroglycan-ligand interactions in congenital muscular dystrophies. Nature **418**:417–422.

46. **Müller, S., R. Geffers, and S. Gunther.** 2007. Analysis of gene expression in Lassa virus-infected HuH-7 cells. J. Gen. Virol. **88**:1568–1575.

47. **Nakabayashi, H., K. Taketa, K. Miyano, T. Yamane, and J. Sato.** 1982. Growth of human hepatoma cells lines with differentiated functions in chemically defined medium. Cancer Res. **42**:3858–3863.

48. **Nichols, B. J.** 2002. A distinct class of endosome mediates clathrin-independent endocytosis to the Golgi complex. Nat. Cell Biol. **4**:374–378.

49. **Oh, P., D. P. McIntosh, and J. E. Schnitzer.** 1998. Dynamin at the neck of caveolae mediates their budding to form transport vesicles by GTP-driven fission from the plasma membrane of endothelium. J. Cell Biol. **141**:101–114.

50. **Oldstone, M. B.** 2002. Biology and pathogenesis of lymphocytic choriomeningitis virus infection. Curr. Top. Microbiol. Immunol. **263**:83–117.

51. **Parton, R. G., and A. A. Richards.** 2003. Lipid rafts and caveolae as portals for endocytosis: new insights and common mechanisms. Traffic **4**:724–738.

52. **Pelkmans, L., T. Burli, M. Zerial, and A. Helenius.** 2004. Caveolin-stabilized membrane domains as multifunctional transport and sorting devices in endocytic membrane trafficking. Cell **118**:767–780.

53. **Pelkmans, L., J. Kartenbeck, and A. Helenius.** 2001. Caveolar endocytosis of simian virus 40 reveals a new two-step vesicular-transport pathway to the ER. Nat. Cell Biol. **3**:473–483.

54. **Pelkmans, L., D. Puntener, and A. Helenius.** 2002. Local actin polymerization and dynamin recruitment in SV40-induced internalization of caveolae. Science **296**:535–539.

55. **Perez, M., R. Clemente, C. S. Robison, E. Jeetendra, H. R. Jayakar, M. A. Whitt, and J. C. de la Torre.** 2007. Generation and characterization of a recombinant vesicular stomatitis virus expressing the glycoprotein of Borna disease virus. J. Virol. **81**:5527–5536.

56. **Perez, M., M. Watanabe, M. A. Whitt, and J. C. de la Torre.** 2001. N-terminal

57. **Pietiäinen, V., V. Marjomaki, P. Upla, L. Pelkmans, A. Helenius, and T. Hyypia.** 2004. Echovirus 1 endocytosis into caveosomes requires lipid rafts, dynamin II, and signaling events. Mol. Biol. Cell **15**:4911–4925.

58. **Radoshitzky, S. R., J. Abraham, C. F. Spiropoulou, J. H. Kuhn, D. Nguyen, W. Li, J. Nagel, P. J. Schmidt, J. H. Nunberg, N. C. Andrews, M. Farzan, and H. Choe.** 2007. Transferrin receptor 1 is a cellular receptor for New World haemorrhagic fever arenaviruses. Nature **446**:92–96.

59. **Robison, C. S., and M. A. Whitt.** 2000. The membrane-proximal stem region of vesicular stomatitis virus G protein confers efficient virus assembly. J. Virol. **74**:2239–2246.

60. **Rodal, S. K., G. Skretting, O. Garred, F. Vilhardt, B. van Deurs, and K. Sandvig.** 1999. Extraction of cholesterol with methyl-beta-cyclodextrin perturbs formation of clathrin-coated endocytic vesicles. Mol. Biol. Cell **10**:961–974.

61. **Rojek, J. M., C. F. Spiropoulou, K. P. Campbell, and S. Kunz.** 2007. Old World and clade C New World arenaviruses mimic the molecular mechanism of receptor recognition used by α-dystroglycan's host-derived ligands. J. Virol. **81**:5685–5695.

62. **Rose, J. K., and M. A. Whitt.** 2001. Rhabdoviridae: the viruses and their replication, p. 1221–1244. *In* B. N. Fields and D. M. Knipe (ed.), Fields virology, 4th ed. Lippincott-Raven, Philadelphia, PA.

63. **Sánchez, A. B., M. Perez, T. Cornu, and J. C. de la Torre.** 2005. RNA interference-mediated virus clearance from cells both acutely and chronically infected with the prototypic arenavirus lymphocytic choriomeningitis virus. J. Virol. **79**:11071–11081.

64. **Schmid, S. L., and L. L. Carter.** 1990. ATP is required for receptor-mediated endocytosis in intact cells. J. Cell Biol. **111**:2307–2318.

65. **Schnell, M. J., L. Buonocore, E. Kretzschmar, E. Johnson, and J. K. Rose.** 1996. Foreign glycoproteins expressed from recombinant vesicular stomatitis viruses are incorporated efficiently into virus particles. Proc. Natl. Acad. Sci. USA **93**:11359–11365.

66. **Shah, W. A., H. Peng, and S. Carbonetto.** 2006. Role of non-raft cholesterol in lymphocytic choriomeningitis virus infection via α-dystroglycan. J. Gen. Virol. **87**:673–678.

67. **Sieczkarski, S. B., and G. R. Whittaker.** 2002. Influenza virus can enter and infect cells in the absence of clathrin-mediated endocytosis. J. Virol. **76**:10455–10464.

68. **Simons, K., and W. L. Vaz.** 2004. Model systems, lipid rafts, and cell membranes. Annu. Rev. Biophys. Biomol. Struct. **33**:269–295.

69. **Smith, A. E., and A. Helenius.** 2004. How viruses enter animal cells. Science **304**:237–242.

70. **Spiropoulou, C. F., S. Kunz, P. E. Rollin, K. P. Campbell, and M. B. Oldstone.** 2002. New World arenavirus clade C, but not clade A and B viruses, utilizes α-dystroglycan as its major receptor. J. Virol. **76**:5140–5146.

71. **Stang, E., J. Kartenbeck, and R. G. Parton.** 1997. Major histocompatibility complex class I molecules mediate association of SV40 with caveolae. Mol. Biol. Cell **8**:47–57.

72. **Subtil, A., I. Gaidarov, K. Kobylarz, M. A. Lampson, J. H. Keen, and T. E. McGraw.** 1999. Acute cholesterol depletion inhibits clathrin-coated pit budding. Proc. Natl. Acad. Sci. USA **96**:6775–6780.

73. **Sun, X., V. K. Yau, B. J. Briggs, and G. R. Whittaker.** 2005. Role of clathrin-mediated endocytosis during vesicular stomatitis virus entry into host cells. Virology **338**:53–60.

74. **Takada, A., C. Robison, H. Goto, A. Sanchez, K. G. Murti, M. A. Whitt, and Y. Kawaoka.** 1997. A system for functional analysis of Ebola virus glycoprotein. Proc. Natl. Acad. Sci. USA **94**:14764–14769.

75. **Thorp, E. B., and T. M. Gallagher.** 2004. Requirements for CEACAMs and cholesterol during murine coronavirus cell entry. J. Virol. **78**:2682–2692.

76. **van der Bliek, A. M., T. E. Redelmeier, H. Damke, E. J. Tisdale, E. M. Meyerowitz, and S. L. Schmid.** 1993. Mutations in human dynamin block an intermediate stage in coated vesicle formation. J. Cell Biol. **122**:553–563.

77. **Weber, E. L., and M. J. Buchmeier.** 1988. Fine mapping of a peptide sequence containing an antigenic site conserved among arenaviruses. Virology **164**:30–38.

78. **Yancey, P. G., W. V. Rodrigueza, E. P. Kilsdonk, G. W. Stoudt, W. J. Johnson, M. C. Phillips, and G. H. Rothblat.** 1996. Cellular cholesterol efflux mediated by cyclodextrins. Demonstration of kinetic pools and mechanism of efflux. J. Biol. Chem. **271**:16026–16034.

79. **Yarar, D., C. M. Waterman-Storer, and S. L. Schmid.** 2005. A dynamic actin cytoskeleton functions at multiple stages of clathrin-mediated endocytosis. Mol. Biol. Cell **16**:964–975.

80. **York, J., and J. H. Nunberg.** 2006. Role of the stable signal peptide of Junin arenavirus envelope glycoprotein in pH-dependent membrane fusion. J. Virol. **80**:7775–7780.